Aged boreal biomass burning aerosol size distributions from BORTAS 2011

K.M. Sakamoto[1,2], J. D. Allan[3], H. Coe[3], J. W. Taylor[3], T. J. Duck[2], J. R. Pierce[1,2]

[1] Colorado State University, Fort Collins, CO, USA

[2] Department of Physics and Atmospheric Science, Dalhousie University, Halifax, NS, CAN

[3] University of Manchester, Manchester, UK

Corresponding author: J.R. Pierce (jeffrey.pierce@colostate.edu)

Abstract

Biomass-burning aerosols contribute to aerosol radiative forcing on the climate system. The magnitude of this effect is partially determined by aerosol size distributions, which are functions of source fire characteristics (e.g. fuel type, MCE) and in-plume microphysical processing. The uncertainties in biomass-burning emission number size-distributions in climate model inventories lead to uncertainties in the CCN concentrations and forcing estimates derived from these models.

The BORTAS-B measurement campaign was designed to sample boreal biomass-burning outflow over Eastern Canada in the summer of 2011. Using these BORTAS-B data, we implement plume criteria to isolate the characteristic size-distribution of aged biomass-burning emissions (aged ~ 1 – 2 days) from boreal wildfires in Northwestern Ontario. The composite median size-distribution yields a single dominant accumulation mode with D_{pm} = 230 nm (number-median diameter) and σ = 1.5, which are comparable to literature values of other aged plumes of a similar type. The organic aerosol enhancement ratios ($\Delta OA/\Delta CO$) along the path of Flight b622 show values of 0.09-0.17 $\mu g\ m^{-3}$ $ppbv^{-1}$ with no significant trend with distance from the source. This lack of enhancement ratio increase/decrease with distance suggests no detectable net OA production/evaporation within the aged plume over the sampling period (plume age: 1-2 days), though does not preclude OA production/loss at earlier stages.

A Lagrangian microphysical model was used to determine an estimate of the freshly emitted

size distribution corresponding to the BORTAS-B aged size-distributions. The model was restricted to coagulation and dilution processes based on the insignificant net OA production/evaporation derived from the ΔOA/ΔCO enhancement ratios. We estimate that the young-plume median diameter was in the range of 59-94 nm with modal widths in the range of 1.7-2.8 (the ranges are due to uncertainty in the entrainment rate). Thus, the size of the freshly emitted particles is relatively unconstrained due to the uncertainties in the plume dilution rates.

1. Introduction

1.1 Biomass burning particles

Biomass burning is a significant emission source of carbonaceous aerosols to the global atmosphere (Andreae and Merlet, 2001; Reid et al., 2005). In addition to releasing high levels of greenhouse gases (CO_2, CO) and volatile organic compounds, biomass burning releases smoke particles that have climate impacts through the direct and indirect aerosol effects. These particles are primarily composed of a mixture of black carbon and organic carbon, with inorganics contributing some mass (Capes et al., 2008; Carrico et al., 2010; Cubison et al., 2011; Hecobian et al., 2011; Hennigan et al., 2011; Hudson et al., 2004; Reid et al., 2005). These particles directly affect the Earth's radiation balance and climate by scattering and absorbing incoming solar radiation (Haywood, 2000; Jacobson, 2001). Biomass burning particles may also act as cloud condensation nuclei (CCN) and affect climate and radiation through modifying cloud albedo and lifetime (Pierce et al., 2007; Spracklen et al., 2011) (indirect aerosol effects). Globally, the direct and indirect climate effects represent the largest uncertainties in radiative forcing as quantified by the recent IPCC report (Myhre et al., 2013), and biomass burning emissions represent significant contributions to each of the effects globally (Alonso-Blanco, 2014; Lee et al., 2013).

The size of biomass-burning particles (and all particles in general) can have large impacts on the magnitude of these direct and indirect effects (Lee et al., 2013; Seinfeld and Pandis, 2006; Spracklen et al., 2011). Regarding the direct effect, the mass-scattering and mass-absorption efficiencies (the amount of scattering and absorption per mass of aerosol particles) depend on the size of the particles, so errors in the predicted/assumed values of biomass-burning particle size may lead to errors in simulated direct aerosol climate effects (Seinfeld and Pandis, 2006). Regarding the indirect effect, particles that are larger in diameter and more hygroscopic are more likely to act as CCN (Petters and Kreidenweis, 2007). Typically particles larger than 30-100 nm act as CCN depending on

conditions and hygroscopicity (Petters and Kreidenweis, 2007; Petters et al., 2009), though this range may be slightly larger or smaller for fresh biomass-burning particles due to these particles being initially more hydrophobic/hydrophilic (depending on fuel type) than typical ambient aerosol (Carrico et al., 2010; Engelhart et al., 2012; Petters and Kreidenweis, 2007). Furthermore, for constant emissions mass, a factor-of-2 change in diameter leads to a factor-of-8 change in number emissions, which may contribute to significant changes in CCN concentrations (Pierce et al., 2007; Spracklen et al., 2011). Thus, it is important to provide accurate emissions sizes from biomass burning sources to atmospheric aerosol models looking at aerosol-climate interactions. Lee et al. (2013) found that uncertainties in biomass-burning aerosol emission diameter were responsible for large uncertainties in CCN concentrations in the GLOMAP model (third largest CCN sensitivity out of 28 globally).

Atmospheric processing causes the physical and chemical properties of biomass-burning (BB) aerosol evolve over time. These processes have an effect on the size and composition of the particles, and thus influence their direct and indirect effects. Coagulation is a driving factor in size-distribution evolution due to the high concentrations of particles within plumes (Andreae and Merlet, 2001; Capes et al., 2008). Production of secondary organic aerosol (SOA) in-plume has been observed in chamber studies (Cubison et al., 2011; Grieshop et al., 2009; Hennigan et al., 2011; Heringa et al., 2011; Ortega et al., 2013) and in the field (DeCarlo et al., 2010; Lee et al., 2008; Reid et al., 1998; Yokelson et al., 2009), and this SOA will condense onto the particles growing them to larger sizes. In addition, the primary organic aerosol (POA) emitted by the fires may evaporate during the dilution of the plume (Huffman et al., 2009; May et al., 2013). Finally, new particle formation in smoke plumes has been observed in smog chamber studies (Hennigan et al., 2012) as well as in the field (Andreae et al., 2001; Hobbs et al., 2003; Rissler et al., 2006).

In global and regional modeling of biomass-burning aerosols, mass-based biomass-burning inventories are the standard, and are generally not accompanied by size data (Reid et al., 2009; van der Werf et al., 2010; Wiedinmyer et al., 2011), leaving size-distribution estimates to the individual investigator. Current global and regional atmospheric aerosol models have gridbox spatial scales (10s-100s of kms) much larger than many initial biomass-burning plume widths (<10 km). This means that sub-grid aging of aerosol plumes by microphysical processes (coagulation, condensation/evaporation and nucleation) will lead to changes in the size distribution that the models cannot explicitly resolve. Therefore, the biomass-burning emissions size distributions must be aged distributions that already account for sub-grid processes. Quantifying the natural variations in

biomass-burning aerosols are therefore necessary for accurate predictions. Previous studies of field and lab experiments show biomass burning size-distributions vary according to plume age, combustion phase, and fuel type (Adler et al., 2011; Capes et al., 2008; Hobbs et al., 2003; Hosseini et al., 2010; Janhäll et al., 2010; Okoshi et al., 2014). A review of observed size distribution data by Janhäll et al. (2010) shows the differences in modal width and median diameter as a function of fuel type (forest, savannah, grass), modified combustion efficiency, and plume age (fresh versus aged). Combustion chamber experiments in the FLAME lab have demonstrated similar fuel-type differences in fresh BB size-distributions (Levin et al., 2010).

Due to the combination of emission and atmospheric processing factors contributing to the evolution of the BB aerosol size-distribution, characterization of observed, aged BB aerosol is valuable. Adding to the database of observations helps constrain the uncertainties associated with aerosol size. Thus, to improve biomass-burning-aerosol/climate interactions in models, there is a need to characterize the size of particles in aging and aged biomass-burning plumes for a range of fire types and atmospheric conditions (Bauer et al., 2010; Chen et al., 2010; Lee et al., 2013; Pierce et al., 2007; Reddington et al., 2011; Spracklen et al., 2011). In this paper, we specifically investigate the size distributions measured in aged plumes (1-2 days) of large boreal forest fires over Canada.

In this paper, we analyze size-distribution and organic aerosol data from BORTAS-B flights that sampled highly concentrated smoke plumes over Eastern Canada on July 20-21st, 2011. A brief overview of the BORTAS-B campaign, instrumentation, and source fire conditions are provided in Section 2.1-2.2. A description of the quantitative plume criteria used to determine plume (versus out of plume) sampling periods is found in Section 2.3. In addition to observational data, we use an aerosol-microphysics box model to simulate the microphysical evolution of number size-distributions. This model was employed to estimate the likely young-plume size distribution associated with the source fires sampled by BORTAS-B. A full model description is provided in Section 2.4. We present the BORTAS-B research flight results in Section 3, which include the measured aged size distributions, evidence for/against net OA production, and the aging simulations. Finally, we provide conclusions in Section 4.

2. Methods

2.1 BORTAS overview

The *Quantifying the impact of BOReal forest fires on the Tropospheric oxidants over the Atlantic using*

Aircraft and Satellites (BORTAS-B) measurement campaign was held in Eastern/Atlantic Canada from July 11 – August 3, 2011 (Palmer, 2013). The goal was to characterize pyrogenic outflow from boreal forest wildfires using a variety of sampling and observational techniques with emphasis on plume photochemical evolution.

BORTAS-B incorporated predictive chemical transport modelling (GEOS-Chem), satellite observations, a ground-based in-situ network of sondes (Environment Canada) and ground-base samplers and profilers (Dalhousie Ground Station, DGS), and the UK Facility for Airborne Atmospheric Measurements Airborne Research Aircraft (FAAM-ARA) for inflight sampling. For a complete overview of the BORTAS-B set-up and instrumentation, see (Palmer, 2013). The ARA flew fourteen research flights over the campaign period.

The flight paths of the ARA flights that we analyze in this paper can be seen in Figure 1. Flights BAE-b622 and BAE-b623 were research flights between Halifax, NS and Sherbrooke, QB spanning July 20-21, 2011. They flew ascent and descent patterns (ranging ~1-7 km ASL) to sample vertical and horizontal transects in regions forecasted to contain biomass-burning plumes. These flights were selected because they were roughly co-located and back-to-back, increasing the likelihood of sampling similar outflow and allowing for a common plume criteria to be applied across both flights. They also contained the majority of the biomass-burning aerosol sampled during the 14-flight campaign.

In addition, Flight b622 sampled along a relatively straight path to/from the fires that allowed for analysis of the evolution of plume aerosol properties (Flight b623 had a much more complicated and compact sampling path so we did not use this flight to determine the evolution of aerosol properties). We have divided these flights into vertical transects by ascent/descent with the midpoints transect represented in Figure 1.

The sampled wildfire plumes originated from intense regional fires near the Northwestern Ontario-Manitoba border (centred 52° N, 93° W). The MODIS hotspots in Figure 1 show a number of intense fires (fire radiative power >100 MW) in northwestern Ontario for the three days prior to the analyzed flights (June 17-20, 2011). According to the Ontario Ministry of Natural Resources, Ontario experienced one of its worst fire seasons in terms of burned area with 635,374 hectares burned in 2011. The abundance of individual fires in a relatively large source region led to mixed combustion phases and dominant hotspots over the course of the campaign. A combination of flaming and smouldering phases were reported by Natural Resources Canada with primary fuels consisting of jack pine (*pinus banksiana*) and black spruce (*picea mariana*) throughout the fire region (Ontario ministry of natural

155 resources: 2011 forest summary).

156 The dominant west-east climatological meteorology during the BORTAS-B campaign allowed
157 the biomass-burning emissions from these fires to be transported downwind over the ground-base
158 (DGS) in Halifax, NS (44.5° N, 63.1° W). The plumes intersected by flights b622 and b623 had a
159 physical transport age estimated through HYSPLIT backtrajectories of between 1-2 days as
160 summarized in Table 1. The backtrajectory analysis (not shown) shows air masses passing over the
161 biomass-burning region later being intersected by the flight paths at varying altitudes. The estimated
162 photochemical age of the plumes, calculated by Palmer et al. (2013) (by non-methane hydrocarbon
163 analysis; Parrish et al. (2007)), were 1-5 days for b622 and 2-4 days for b623. These estimates may be
164 longer than the physical transport ages due to the entrainment of background air (which is more
165 photochemically aged) into the plumes.

166

167 ## *2.2 ARA Instrumentation*

168 The ARA aircraft was outfitted with instruments designed for sampling chemical and physical
169 characteristics of biomass-burning outflow. Gaseous and particulate in-flight sampling was
170 accomplished across a suite of instruments; the relevant instruments for this study are described below.
171 A full description of all payload instruments can be found in (Palmer, 2013).

172 The suite of instruments on the ARA included measurements of multiple gaseous
173 biomass-burning tracers. Carbon monoxide (CO) mole fraction was measured via VUV Fast
174 fluorescence CO analyzer averaged over 1s (3% estimated accuracy). Acetonitrile (CH_3CN), a
175 biomass-burning marker VOC associated with plant pyrolysis, was measured along with a number of
176 other VOCs with a proton-transfer-reaction mass spectrometer (PTR-MS) system (co: University of
177 East Anglia). The PTR-MS concentrations were averaged over 1s with an estimated precision of ± 37
178 ppt (Palmer, 2013).

179 Aerosol composition measurements used here were taken by i) refractory black carbon (BC)
180 mass and number measurements from a Single Particle Soot Photometer (SP2) (accuracy 20%,
181 precision 5%, 5s averaging time) and ii) non-refractory organic aerosol (OA) via an aerosol mass
182 spectrometer (precision ~ 15-150 ng m^{-3}) both operated by the University of Manchester (Jolleys et al.
183 2014; Taylor et al., 2014). The number concentrations of the combined aerosol particles was measured
184 by Scanning Mobility Particle Sizer (SMPS) with 26 lognormally-spaced diameter bins ranging from
185 20-330 nm and corrected to STP. A full scan takes 60s (Palmer, 2013). The SMPS data was inverted

using the commonly-used Wiedensohler (1988) parameterisation, however recent work has suggested that this may be quantitatively unreliable for applications to aircraft data due to variations in the charging efficiency with pressure (López-Yglesias and Flagan, 2013; Leppä et al., 2014). While this may have affected the magnitude of the number concentrations, no altitude dependency was noted in the sizing data, so the conclusions of this paper regarding particle size are unaffected.

The combination of gas and particle tracer measurements listed above were used to identify flight periods of biomass-burning plume sampling, determine if SOA formation or OA evaporation may have occurred in the plume, and characterize the size-distribution of aerosols within the plume.

2.3 Plume Criteria

We determine if measurements are in-plume versus out-of-plume using threshold plume criteria. We designate sampling periods as in-plume if pre-specified threshold values of four tracer species: CO, CH_3CN, BC, and OA, were exceeded. For out-of-plume conditions, we determine "background values" for each tracer by averaging the tracers over the out-of-plume periods.

Carbon monoxide (τ_{co} ~ months (Staudt et al., 2001)) and acetonitrile (τ_{ace} ~ 6 months (Holzinger et al., 2005)) were used in conjunction as gaseous tracers due to their high mixing ratios in biomass-burning plumes relative to the background and long atmospheric lifetimes relative to the estimated plume transport times. The background CO levels were 80-120 ppbv with an overall average of 100 ppbv. The threshold CO value was set to 150 ppbv (1.5 x [background]), with some CO concentrations in-plume reaching ten times background concentrations (1000 ppbv). The threshold CH_3CN level was 200 pptv (background ~ 100 pptv).

The particulate matter thresholds (BC number, OA mass) were introduced to ensure high-enough aerosol contributions to the plume to analyze size-distributions. This ensured high-gas, low-aerosol sampling periods were not included in the size-distribution analysis. At least one case of this situation in BORTAS-B has been attributed by Franklin et al. (2014) to aerosol rainout during transport. The mean background concentrations for both BC number and OA mass were minimal (< 20 cm^{-3} and 2 $\mu g\ m^{-3}$ respectively). The threshold values were set to 50 cm^{-3} for BC number and 20 $\mu g\ m^{-3}$ for OA mass. These thresholds for particles are higher relative to background than CO and CH_3CN because we wanted to exclude a higher-elevation plume that had undergone aerosol wet deposition (see Section 3.2).

The selected CO, CH_3CN, aerosol data, and flight altitude time series for Flight b622 is shown

in Figure 2. The flight is divided into transects (labeled 1-9 and colored) as seen in the altitude plot (Figure 2, bottom). We use these in-plume time periods to differentiate between in-plume and background aerosols throughout the paper.

2.4 Model Description

We use a Lagrangian box model to simulate the evolution of the biomass-burning size distribution due to coagulation. The model has fifty-five logrithmically distributed size bins that correspond to the size bins of the SMPS on the ARA and extend to both larger and smaller diameters. The model includes coagulation and dilution as the only physical processes, with no chemistry or speciation of the aerosol (we show in Section 3.2 that we cannot see evidence of net OA condensation/evaporation in the plume over the sampling period). The model distributions are therefore limited by the lack of condensational growth known to occur in BB plumes during the first few hours of aging (e.g. Reid et al. 1998).

We use an inverse method to estimate the initial young (~ 1 hour) size-distributions by successively running the model from initial conditions to BORTAS observation forward in time and changing the initial size distribution until the model most closely matches the observed aged size distribution. This method estimates the initial distribution assuming that coagulation was the only physical processes affecting the in-plume particles. The box model does not include any cloud interaction chemistry, which could have influenced the distribution considerably depending on meteorological conditions, notably through wet deposition and aqueous chemistry.

Each model forward simulation requires the young size-distribution input as a single lognormal mode with parameters: median diameter (D_{pm}), modal width (σ), and particle number (N_0). For coagulation, we use the brownian coagulation kernel of Fuchs (1964). Dilution of the plume in transport was modelled using a simple e-folding volume mixing time, τ_{dil}. This parameter controlled the entrainment each timestep between the in-plume and background aerosol. The rate of plume dilution may significantly affect the rate of coagulation throughout the simulation (the coagulation rate is proportional to N^2). Different values of τ_{dil} were tested to account for a range of entrainment rates as the dilution rate in the plume is relatively unconstrained. We test τ_{dil} values of 24, 36 and 48 hours. The 36 hr dilution timescale was calculated as the mean timescale for dilution from Gaussian plume equations with an initial plume width of 10 km in a neutral stability environment (Klug, 1969) (note, however, that expansion occurs at faster timescales early in the plume aging, and this timescale slows with time). The range (24 – 48 hrs) accounts for atmospheric stability and plume width variations in the BORTAS

source region. The model simulation time is 48 hours based on the upper age limits shown in Table 1.

To determine the best estimate for initial conditions, we simulate a range of young plume parameters: median diameter, D_{pm}, modal width, σ, and number, N_0. The input median diameter range was between 60-120 nm (increment = 1 nm), with σ ranging from 1.0-2.5 (increment = 0.1) and N_0 ranging from 5,000- 150,000 cm^{-3} (increment = 500 cm^{-3}). The parameter space was optimized by brute force (i.e. every combination of input parameters was simulations) for each set dilution time and the final modelled size-distribution was compared to the observed in-plume size distribution by an equally weighted objective function. The objective function used was the sum of the absolute residual across the SMPS range. Modelled data outside of the SMPS size range was not used in the objective function.

3. Results

3.1 Observed size distributions

Observed SMPS size-distributions for individual plume transects showed highly elevated particle counts with little variation between transects and flights. The transect-divided data for Flight b622 are shown in Figure 3. Transects 2-6 and 9, show a clearly elevated accumulation mode within the plume, with peak median diameters of 180-240 nm. Transects 1, 7 and 8 have significantly less data (< 3 data points per size bin) due to the lesser in-plume sampling periods (incomplete SMPS scans).

Those transects with sufficient plume data (> 3 data points per bin) are plotted against their accumulation mode median diameter D_{pm} in Figure 4. We do not observe any discernible trend in size-distribution with the distance from the source fires in either median diameter or number concentration. This lack of a trend suggests that the microphysical processing during the range of distances sampled has smaller effects on the size distribution than the variability between plumes for Flight b622. Similarly small inter-transect variation was seen for Flight b623 (not shown). The median size-distributions show no bias based on altitude or ascent/descent rate as an artefact of SMPS flow rate fluctuations from altitude changes (not shown).

The composite median distribution across all plume sampling periods and both flights is shown in Figure 5a. This characteristic size distribution is presented as a median value, minimizing the contributions of outlying data. Figure 5b shows the same composite distribution normalized by CO concentration to attempt to account for differences in the amount of emissions from the source. The plume particle size-distribution shows the median size distribution highlighted in black, with the 25th

and 75th percentiles outlined in red. A clearly defined accumulation mode was identified centred at D_{pm} = 230 nm and with a modal width of 1.5, based on a single lognormal mode fit. Normalizing the plume distribution by CO mixing ratio produced a very similar pattern shown in Figure 5b (accumulation mode: D_{pm} = 230 nm, σ = 1.4). The composite background aerosol size-distribution (sampling periods that failed the in-plume criteria) are seen in black (with 25th and 75th percentiles shown in gray) in Figure 5a. It shows relatively constant $dN/dlogD_p$ concentrations across the SMPS range and is lacking the concentrated accumulation mode found in-plume.

The aged composite size-distribution and associated lognormal parameters are similar to those found in other field studies of aged biomass-burning emissions. Aged biomass-burning size distributions compiled by Janhäll et al. (2010) for all different fuel types show a similar D_{pm} to modal width ratio (D_{pm} = 175 – 300 nm, σ = 1.7 – 1.3). Capes et al. (2008) show a similar aged BB size distribution median diameter over West Africa during the DABEX campaign (D_{pm} = 240 nm). The ARCTAS-B campaign over Northern Canada sampled similar Boreal pyrogenic outflow and collected very similar aged distributions of BC and OC constituents (D_{pm} = 224 ± 14 nm, σ = 1.33 ± 0.05) (Kondo et al., 2011).

Of note in the BORTAS-B plume size distribution is the elevated number concentrations of small diameter particles (20-90 nm), which form an elevated small-diameter 'tail' of the distribution. These higher concentrations were not expected due to the high rate of removal of small particles by coagulation with the larger particles in the accumulation mode. We calculated first-order coagulational-loss timescales to investigate the timescale of the removal of these small particles by the larger plume particles. If these small particles were brought into the plume by entrainment of background air, there would be an associated amount of time before these particles were lost by coagulation. For the calculation, we assume brownian coagulation of entrained background aerosol (bin range 20-90 nm) with the observed in-plume SMPS data (90-333 nm) and with artificial large-diameter bins from 330 nm – 1 um (6 bins). These artificial bin concentrations were based on the accumulation mode lognormal fit and account for those particle concentrations at sizes larger than those measured by the SMPS but that nonetheless contribute to the coagulational scavenging of the small-diameter particles. Particles with diameters > 1 μm were ignored since their relative scarcity relative to the large number of accumulation-mode particles causes a negligible impact on the number-concentration driven coagulation process.

The predicted concentrations of background aerosol remaining after 24, 36 and 48 hours are

shown in Figure 6a. These times are within the estimated physical transport age ranges of the transects. After 12 hours, coagulation alone has already caused a significant decrease in the concentrations of the smallest measured particles, reducing them to levels well below the concentrations observed in plume (red line). This deficit increases with time (t=36 hrs, t=48 hrs). The coagulation lifetimes of the particles in this diameter range (30-90 nm) are seen in Figure 6b and extend into the tens of hours. Note that the concentrations of these small-diameter particles are similar in the plume compared to the background. This means that the entrainment rate of background air into the plume would need to be much faster than the coagulational loss timescales (~5 hours for 20 nm particles) in order for entrainment to sustain the number of small particles. If entrainment timescales were significantly shorter than 5 hours, the plume would almost completely disperse into the background within 1 day.

There are a number of mechanisms other than entrainment that could explain the higher tail concentrations found in plume despite the short coagulation lifetimes. In-plume nucleation and subsequent growth to SMPS-detectable sizes could also partially account for sustained elevated small particle concentrations. Hennigan et al. (2012) showed with the FLAME-III chamber studies that in-plume nucleation was possible as a result of photochemical aging and SOA production in smoke plumes. Nucleation modes in association with smoke plumes have also been observed previously in field studies (Hobbs et al., 2003; Rissler et al., 2006). We attempted to determine the nucleation and growth rates required to sustain the observed concentration of small particles; however, the necessary condensational growth rates that were required to fit the observed data were unrealistically high, which we see as evidence against nucleation/growth being the primary source of the small particles. Thus, we are unsure of the source of these particles.

3.2 Net production/loss of organic aerosol with time

Enhancement ratios are a way of characterizing plume chemistry as a ratio of a specific species to a reference species. This was done for the sampled BORTAS pyrogenic outflow by taking the excess (background concentration removed) of the AMS organic aerosol normalized to the excess CO ($\Delta OA/\Delta CO$). Only those data which were in excess of the mean background (CO = 100 ppbv, OA = 2 $\mu g\ m^{-3}$) were compiled. The characteristic $\Delta OA/\Delta CO$ ratio can be used as a comparison value between fires of different fuel type, phases or photochemical ages.

Since CO has a sufficiently long lifetime and is co-emitted with OA in abundance at the source, any changes in the organic aerosol enhancement ratio over the lifetime of the plume are attributed to

in-plume chemistry. Entrainment of background air into the most concentrated sections of the plumes is slow (timescale > 10 hours) and we consider any change in ΔOA/ ΔCO ratios to be attributable to in-plume processes only. The formation of secondary organic aerosol is possible within the plume by oxidation of organic vapors to lower-volatility products. Evaporation of less-volatile POA during plume dilution competes with the SOA condensation. The net OA production is therefore: $\Delta OA_{net} = SOA_{prod} - OA_{evap}$. Changes in the ΔOA/ ΔCO ratio over time can therefore indicate which of the two processes is dominant.

The organic aerosol enhancement ratios for Flight b622 are shown in Figure 7. There is a fairly pronounced altitude dependence as seen in Figure 7a, with several high altitude (~ 7 km) samples having fairly low excess organic aerosol, but significant ΔCO (300 ppbv). This trend is featured in Franklin et al. (2014) where the high-altitude plume showed evidence of an aerosol rainout event causing low ΔOA/ΔCO within the plume transected at those high altitudes.

We will focus on the lower-altitude plume where the aerosol was not rained out, so we employ a height cutoff of 4.6 km to restrict the enhancement ratio calculations to lower-altitude, OA-rich plumes least likely to have seen significant reduction in organic aerosol from wet deposition. The mean enhancement ratios by transect are seen in Figure 7b (for transect locations see Figure 1). Only those sampling periods that passed the OA and CO plume criteria (detailed above) are shown. The lower-altitude plume enhancement ratio show correlations of $R^2>0.5$ for each transect with the exception of Transect 8 ($R^2=0.26$).

Figure 8 shows ΔOA/ ΔCO as a function of the distance from the source fires (horizontal error bars correspond to error due to the radius of the Ontario fire region, vertical error bars are calculated from transect data scatter). Compared across transects, the enhancement ratios show no significant trend (to P-value = 0.55). The average enhancement ratio is 0.14 ±0.01 [$\mu g\ m^{-3}\ ppbv^{-1}$] and can be considered characteristic of the aged boreal plume during these BORTAS flights.

The lack of trend in Figure 8 suggests that we cannot determine if there was any net production/evaporation of OA happening inside the plume over this sampling period (plume ages: 1-2 days). Any SOA produced photochemically inside the plume is either being accompanied by an opposing loss of POA or at such a rate that is below the observational variability over the sampled time period. The statistically invariant ΔOA/ ΔCO does not discount evaporation-condensational cycling of POA and SOA, or the effects such recondensation would have on the size-distribution (although there was no apparent trend in the size distribution either [Figure 4]). No increase in normalized excess OA

fraction means significant levels of excess SOA were not likely driving condensational growth, ensuring that coagulation was dominating the size-distribution evolution during the period of aging between 1 day and 2 days since emission.

Since no significant trend was found in size-distribution D_{pm} with distance from the source in the observations (> 1000 km; see Figure 4), any effect of POA-SOA cycling on the shape of the distribution cannot be isolated above the noise. However, it does not preclude that there was significant net OA production/evaporation that occurred prior to or after this observed period as has been observed in other BB field studies (e.g. Akagi et al. (2012)*;* Yokelson et al. 2009).Thus, although evidence of photo-oxidation and chemical processing was observed in-plume by Parrington et al. (2013), any chemical composition impact on the size-distribution at the ages observed here seems negligible.

3.2 Estimation of the young biomass burning size distribution

In this section, we test the parameter space of our microphysical model to estimate the young (aged ~1-3 hr) plume size-distribution emitted from the source fires. We allowed the young biomass-burning size distribution to evolve for 48 hours and compared the result to the observed SMPS plume composite distribution to isolate the optimal young plume size-distribution parameters. These were then compared to observed young BB size distributions for context.

The Lagrangian microphysical model was run for 48 hours with fixed entrainment coefficients of τ_{dil}=24 hrs, τ_{dil} = 36 hours and τ_{dil}=48 hours. Figure 9a shows the optimal young plume distribution parameters that were obtained for each tested entrainment rate (with particle number concentration per co-emitted CO above background). Figure 9b shows the modelled aged distributions plotted with the measured distribution. None of the model runs can capture the elevated concentrations in the tail particles in the SMPS data, though this is expected due to the coagulation-dominant aging in the model (discussed above) and adds further uncertainty to the existence of this small tail.

The young plume size-distributions are unimodal with median diameters of 94 nm, 67 nm, and 59 nm for τ_{dil} =24 hrs, τ_{dil}=36 hrs and τ_{dil}=48 hrs, respectively (σ = 1.7, 2.1, 2.8, respectively). The higher entrainment rate of background aerosol requires the young plume distribution to be narrower (lower σ) and have an initial median diameter closer to the final diameter (D_{pfinal} = 230 nm). The initial number concentrations in the young plume were found to be optimized at 62,500, 80,000, and 115,000 [cm^{-3}] for τ_{dil}=48 hrs, τ_{dil}=36 hrs and τ_{dil}=24 hrs, respectively. The initial higher concentrations, narrower

403 modal width and larger median diameter are required for the higher entrainment rates to account for the
404 more rapid plume dilution and subsequently the slowing of the coagulation rates. Normalized to
405 estimated freshly emitted excess CO, the young plume number concentrations are 37, 53, and 60 cm^{-3}
406 $ppbv^{-1}$ (for τ_{dil}=24 hrs, τ_{dil}=36 hrs and τ_{dil}=48 hrs respectively; see Figure 9a). The similar magnitudes of
407 these normalized size-distributions indicate a relatively robust particle/CO ratio regardless of the
408 dilution parameter, though in the absence of the source fire fuel densities, a direct comparison to
409 emission factors (kg^{-1}) cannot be made.
410 As the exact aging time and dilution profiles are unknown in addition to uncertainties in the
411 plume age, we cannot say with certainty which of these estimates is best; however, these results
412 compare to the field observations presented in Janhäll et al. (2010) for fresh plume smoke (range: D_{pm} =
413 100-150 nm) and to small-scale lab experiments measuring fresh smoke (range: D_{pm} = 30-90 nm)
414 (Hosseini et al., 2010). Capes et al. (2008) conducted a similar fresh-plume size-distribution estimate
415 from their observed DABEX aged African smoke data using a coagulation box-model without dilution.
416 Their estimates for very fresh smoke have a much smaller D_{pm} (~ 30 nm).
417 The plume size distributions modelled here are very sensitive to microphysical processes
418 directly after emission. Very close to the source, rapid dilution and condensation (due to cooling) may
419 occur, which are not captured by the coagulation/dilution model we have developed. Thus the
420 modelled plumes are better categorized as 'young' rather than freshly emitted. The young-plume
421 distributions in this study neglect any immediate effects of condensation and/or evaporation of OA on
422 the size-distribution during cooling and dilution respectively, and focus on the effects of coagulation
423 which shape the size-distribution over a longer timescale (~ 10hrs). There is therefore an associated
424 uncertainty in the young distributions due to the exclusion of condensational growth from the model,
425 despite evidence of its effects on BB particle sizes especially during the first hours of aging (e.g. Reid
426 et al. 1998).
427 Figure 10 shows a time series of the optimal modelled size distribution for τ_{dil} = 36 hrs over the
428 48 hr period. The median diameter growth (black line) occurs more rapidly during the early stages of
429 the plume due to the higher particle concentrations before significant dilution. Eighty percent of the
430 final median diameter is achieved within 10 hrs of coagulation processing. Less drastic but similar
431 rapid growth by coagulation was seen by Capes et al. (2008) in their coagulation box model. This quick
432 size distribution evolution within the early plume stages suggests that large grid box models (global,
433 regional) should be using aged biomass-burning size-distributions as input. Figure 10 also shows the

size-distribution growth slowing considerably as the particle concentrations decrease and perhaps can provide an explanation for the lack of strong trend in the observed BORTAS D_{pm} across transects (Figure 4), which were already aged between 1-2 days when they were sampled.

4. Conclusions

The BORTAS-B campaign provided the opportunity to collect numerous gaseous and aerosol measurements from aged North-American biomass-burning plumes in July, 2011. The boreal fire emissions in northwestern Ontario were transported (1-2 days) downwind to where they were sampled by the FAAM BAE-146 research aircraft. We analyzed the plume data from two research flights (b622 and b623) and found little variation in size-distributions between transects.

A characteristic size-distribution consistent between flights and transects was dominated by the accumulation mode with D_{pm} = 230 nm and with σ = 1.5. This unimodal result is consistent with aged biomass-burning observations found globally in the previous field studies (Capes et al., 2008; Janhäll et al., 2010; Kondo et al., 2011).

We also found elevated concentrations of small-diameter particles in the plume contrary to their coagulation lifetimes associated with the biomass-burning-associated accumulation mode. We were not able to explain such concentrations by entrainment of background aerosol alone. The presence of such concentrations in the size-distribution tail remains inconclusive.

The ΔOA/ ΔCO enhancement ratios across Flight b622 show a strong linear correlation below 4.6 km (R^2>0.50) with values between (0.09 – 0.17) ± 0.01 μg m^{-3} $ppbv^{-1}$. We found no trend in transect enhancement ratios with distance from the source, indicating no significant net SOA production in-plume over the sampling period, though this does not preclude OA production or loss during earlier stages of aging.

We used a microphysical model to estimate the young plume size distribution associated with the BORTAS-B observations. Optimizing lognormal parameters for different assumed dilution coefficients (τ_{dil} = 24, 36, 48 hrs), the young plume size distribution had D_{pm} = 59-94 nm, σ = 2.8-1.7, and N_0 = 62,500 – 115,000 cm^{-3} (37 – 60 $cm^{-3}ppbv^{-1}$ normalized by initial co-emitted excess CO). Though the model lacks condensation and chemical considerations, processing through coagulation and dilution alone led to 80% of the observed 48-hour median-diameter growth within the first 10 hrs. This suggests that global climate models should be using coagulation-aged BB size distribution inputs to account for the rapid evolution in plume particle size occurring on scales smaller than the gridbox

length.

5. References

Adler, G., Flores, J. M., Abo Riziq, a., Borrmann, S. and Rudich, Y.: Chemical, physical, and optical evolution of biomass burning aerosols: a case study, Atmos. Chem. Phys., 11(4), 1491–1503, doi:10.5194/acp-11-1491-2011, 2011.

Akagi, S. K., Craven, J. S., Taylor, J. W., McMeeking, G. R., Yokelson, R. J., Burling, I. R., Urbanski, S.P., Wold, C. E., Seinfeld, J. H., Coe, H., Alvarado, M. J. and Weise, D. R.: Evolution of trace gases and particles emitted by a chaparral fire in California, Atmos. Chem. Phys., 12(3), 1397–1421,doi:10.5194/acp-12-1397-2012, 2012

Alonso-Blanco, E.: Impact of Biomass Burning on Aerosol Size Distribution, Aerosol Optical Properties and Associated Radiative Forcing, Aerosol Air Qual. Res., 006, 708–724, doi:10.4209/aaqr.2013.05.0163, 2014.

Andreae, M. O. and Merlet, P.: Emission of trace gases and aerosols from biomass burning, Global Biogeochem. Cycles, 15(4), 955–966, doi:10.1029/2000GB001382, 2001.

Andreae, M. O., Artaxo, P., Fischer, H., Freitas, S. R., Grégoire, J.-M., Hansel, A., Hoor, P., Kormann, R., Krejci, R., Lange, L., Lelieveld, J., Lindinger, W., Longo, K., Peters, W., de Reus, M., Scheeren, B., Silva Dias, M. A. F., Ström, J., van Velthoven, P. F. J. and Williams, J.: Transport of biomass burning smoke to the upper troposphere by deep convection in the equatorial region, Geophys. Res. Lett., 28(6), 951–954, doi:10.1029/2000GL012391, 2001.

Bauer, S. E., Menon, S., Koch, D., Bond, T. C. and Tsigaridis, K.: A global modeling study on carbonaceous aerosol microphysical characteristics and radiative effects, Atmos. Chem. Phys., 10(15), 7439–7456, doi:10.5194/acp-10-7439-2010, 2010.

Capes, G., Johnson, B., McFiggans, G., Williams, P. I., Haywood, J. and Coe, H.: Aging of biomass burning aerosols over West Africa: Aircraft measurements of chemical composition, microphysical properties, and emission ratios, J. Geophys. Res., 113, D00C15, doi:10.1029/2008JD009845, 2008.

Carrico, C. M., Petters, M. D., Kreidenweis, S. M., Sullivan, A. P., McMeeking, G. R., Levin, E. J. T., Engling, G., Malm, W. C. and Collett, J. L.: Water uptake and chemical composition of fresh aerosols generated in open burning of biomass, Atmos. Chem. Phys., 10(11), 5165–5178, doi:10.5194/acp-10-5165-2010, 2010.

Chen, W.T., Lee, Y. H., Adams, P. J., Nenes, A. and Seinfeld, J. H.: Will black carbon mitigation dampen aerosol indirect forcing?, Geophys. Res. Lett., 37(9), L09801, doi:10.1029/2010GL042886, 2010.

Cubison, M. J., Ortega, A. M., Hayes, P. L., Farmer, D. K., Day, D., Lechner, M. J., Brune, W. H., Apel, E., Diskin, G. S., Fisher, J. A., Fuelberg, H. E., Hecobian, A., Knapp, D. J., Mikoviny, T., Riemer, D., Sachse, G. W., Sessions, W., Weber, R. J., Weinheimer, A. J., Wisthaler, A. and Jimenez, J. L.: Effects of aging on organic aerosol from open biomass burning smoke in aircraft and laboratory studies, Atmos. Chem. Phys., 11(23), 12049–12064, doi:10.5194/acp-11-12049-2011, 2011.

DeCarlo, P. F., Ulbrich, I. M., Crounse, J., de Foy, B., Dunlea, E. J., Aiken, A. C., Knapp, D.,

505 Weinheimer, A. J., Campos, T., Wennberg, P. O. and Jimenez, J. L.: Investigation of the sources
506 and processing of organic aerosol over the Central Mexican Plateau from aircraft measurements
507 during MILAGRO, Atmos. Chem. Phys., 10(12), 5257–5280, doi:10.5194/acp-10-5257-2010,
508 2010.

509 Engelhart, G. J., Hennigan, C. J., Miracolo, M. A., Robinson, A. L. and Pandis, S. N.: Cloud
510 condensation nuclei activity of fresh primary and aged biomass burning aerosol, Atmos. Chem.
511 Phys., 12(15), 7285–7293, doi:10.5194/acp-12-7285-2012, 2012.

512 Franklin, J. E., Drummond, J. R., Griffin, D., Pierce, J. R., Waugh, D. L., Palmer, P. I., Parrington, M.,
513 Lee, J. D., Lewis, A. C., Rickard, A. R., Taylor, J. W., Allan, J. D., Coe, H., Walker, K. A.,
514 Chisholm, L., Duck, T. J., Hopper, J. T., Blanchard, Y., Gibson, M. D., Curry, K. R., Sakamoto, K.
515 M., Lesins, G., Dan, L., Kliever, J. and Saha, A.: A case study of aerosol scavenging in a biomass
516 burning plume over eastern Canada during the 2011 BORTAS field experiment, Atmos. Chem.
517 Phys., 14(16), 8449–8460, doi:10.5194/acp-14-8449-2014, 2014.

518 Fuchs, N. A.: The Mechanics of Aerosols, Oxford: Pergamon Press., 1964.

519 Grieshop, A. P., Logue, J. M., Donahue, N. M. and Robinson, A. L.: Laboratory investigation of
520 photochemical oxidation of organic aerosol from wood fires 1: measurement and simulation of
521 organic aerosol evolution, Atmos. Chem. Phys., 9(4), 1263–1277, doi:10.5194/acp-9-1263-2009,
522 2009.

523 Haywood, J. and Boucher, O.: Estimates of the direct and indirect radiative forcing due to tropospheric
524 aerosols: a review, Rev. Geophys., 38, 513–543, doi:10.1029/1999RG000078, 2000.

525 Hecobian, A., Liu, Z., Hennigan, C. J., Huey, L. G., Jimenez, J. L., Cubison, M. J., Vay, S., Diskin, G.
526 S., Sachse, G. W., Wisthaler, A., Mikoviny, T., Weinheimer, A. J., Liao, J., Knapp, D. J.,
527 Wennberg, P. O., Kürten, A., Crounse, J. D., Clair, J. St., Wang, Y. and Weber, R. J.: Comparison
528 of chemical characteristics of 495 biomass burning plumes intercepted by the NASA DC-8 aircraft
529 during the ARCTAS/CARB-2008 field campaign, Atmos. Chem. Phys., 11(24), 13325–13337,
530 doi:10.5194/acp-11-13325-2011, 2011.

531 Hennigan, C. J., Miracolo, M. A., Engelhart, G. J., May, A. A., Presto, A. A., Lee, T., Sullivan, A. P.,
532 McMeeking, G. R., Coe, H., Wold, C. E., Hao, W.-M., Gilman, J. B., Kuster, W. C., de Gouw, J.,
533 Schichtel, B. A., Kreidenweis, S. M. and Robinson, A. L.: Chemical and physical transformations
534 of organic aerosol from the photo-oxidation of open biomass burning emissions in an
535 environmental chamber, Atmos. Chem. Phys., 11(15), 7669–7686, doi:10.5194/acp-11-7669-2011,
536 2011.

537 Hennigan, C. J., Westervelt, D. M., Riipinen, I., Engelhart, G. J., Lee, T., Collett, J. L., Pandis, S. N.,
538 Adams, P. J. and Robinson, A. L.: New particle formation and growth in biomass burning plumes:
539 An important source of cloud condensation nuclei, Geophys. Res. Lett., 39(9), n/a–n/a,
540 doi:10.1029/2012GL050930, 2012.

541 Heringa, M. F., DeCarlo, P. F., Chirico, R., Tritscher, T., Dommen, J., Weingartner, E., Richter, R.,
542 Wehrle, G., Prévôt, A. S. H. and Baltensperger, U.: Investigations of primary and secondary
543 particulate matter of different wood combustion appliances with a high-resolution time-of-flight
544 aerosol mass spectrometer, Atmos. Chem. Phys., 11(12), 5945–5957,
545 doi:10.5194/acp-11-5945-2011, 2011.

546 Hobbs, P. V., Sinha, P., Yokelson, R. J., Christian, T. J., Blake, D. R., Gao, S., Kirchstetter, T. W.,

547 Novakov, T. and Pilewskie, P.: Evolution of gases and particles from a savanna fire in South
548 Africa, J. Geophys. Res., 108(D13), doi:10.1029/2002JD002352, 2003.

549 Holzinger, R., Williams, J., Salisbury, G., Klüpfel, T., de Reus, M., Traub, M., Crutzen, P. J. and
550 Lelieveld, J.: Oxygenated compounds in aged biomass burning plumes over the Eastern
551 Mediterranean: evidence for strong secondary production of methanol and acetone, Atmos. Chem.
552 Phys., 5(1), 39–46, doi:10.5194/acp-5-39-2005, 2005.

553 Hosseini, S., Li, Q., Cocker, D., Weise, D., Miller, A., Shrivastava, M., Miller, J. W., Mahalingam, S.,
554 Princevac, M. and Jung, H.: Particle size distributions from laboratory-scale biomass fires using
555 fast response instruments, Atmos. Chem. Phys., 10(16), 8065–8076,
556 doi:10.5194/acp-10-8065-2010, 2010.

557 Hudson, P. K., Murphy, D. M., Cziczo, D. J., Thomson, D. S., de Gouw, J. A., Warneke, C., Holloway,
558 J., Jost, H.-J. and Hübler, G.: Biomass-burning particle measurements: Characteristic composition
559 and chemical processing, J. Geophys. Res., 109(D23), D23S27, doi:10.1029/2003JD004398,
560 2004.

561 Huffman, J. A., Docherty, K. S., Mohr, C., Cubison, M. J., Ulbrich, I. M., Ziemann, P. J., Onasch, T. B.
562 and Jimenez, J. L.: Chemically-Resolved Volatility Measurements of Organic Aerosol from
563 Different Sources, Environ. Sci. Technol., 43(14), 5351–5357, doi:10.1021/es803539d, 2009.

564 Jacobson, M. Z.: Strong radiative heating due to the mixing state of black carbon in atmospheric
565 aerosols, Nature, 409(6821), 695–697, 2001.

566 Janhäll, S., Andreae, M. O. and Pöschl, U.: Biomass burning aerosol emissions from vegetation fires :
567 particle number and mass emission factors and size distributions, Atmos. Chem. Phys, 1427–1439,
568 2010.

569 Klug,W. : A method for determining diffusion conditions from synoptic observations, Staub-Reinhalt.
570 Luft, 29, 14–20, 1969.
571
572 Kondo, Y., Matsui, H., Moteki, N., Sahu, L., Takegawa, N., Kajino, M., Zhao, Y., Cubison, M. J.,
573 Jimenez, J. L., Vay, S., Diskin, G. S., Anderson, B., Wisthaler, A., Mikoviny, T., Fuelberg, H. E.,
574 Blake, D. R., Huey, G., Weinheimer, A. J., Knapp, D. J. and Brune, W. H.: Emissions of black
575 carbon, organic, and inorganic aerosols from biomass burning in North America and Asia in 2008,
576 J. Geophys. Res., 116(D8), D08204, doi:10.1029/2010JD015152, 2011.

577 Jolleys, M. D., Coe, H., McFiggans, G., Taylor, J. W., O'Shea, S. J., Le Breton, M., Bauguitte, S. J.-B.,
578 Moller, S., Di Carlo, P., Aruffo, E., Palmer, P. I. and Lee, J. D.: Properties and evolution of
579 biomass burning organic aerosol from Canadian boreal forest fires, Atmos. Chem. Phys. Discuss.,
580 14(18), 25095–25138, doi:10.5194/acpd-14-25095-2014, 2014.

581 Lee, L. A., Pringle, K. J., Reddington, C. L., Mann, G. W., Stier, P., Spracklen, D. V., Pierce, J. R. and
582 Carslaw, K. S.: The magnitude and causes of uncertainty in global model simulations of cloud
583 condensation nuclei, Atmos. Chem. Phys., 13(17), 8879–8914, doi:10.5194/acp-13-8879-2013,
584 2013.

585 Lee, S., Kim, H. K., Yan, B., Cobb, C. E., Hennigan, C., Nichols, S., Chamber, M., Edgerton, E. S.,
586 Jansen, J. J., Hu, Y., Zheng, M., Weber, R. J. and Russell, A. G.: Diagnosis of aged prescribed
587 burning plumes impacting an urban area., Environ. Sci. Technol., 42(5), 1438–44, 2008.

588 Leppä, J., Mui, W., Grantz, A. M. and Flagan, R. C.: OP10-5, Importance of charger ion properties in

size distribution measurements, International Aerosol Conference, August 28 - September 2, BEXCO, Busan, Korea, 2014.

Levin, E. J. T., McMeeking, G. R., Carrico, C. M., Mack, L. E., Kreidenweis, S. M., Wold, C. E., Moosmüller, H., Arnott, W. P., Hao, W. M., Collett, J. L. and Malm, W. C.: Biomass burning smoke aerosol properties measured during Fire Laboratory at Missoula Experiments (FLAME), J. Geophys. Res., 115(D18), D18210, doi:10.1029/2009JD013601, 2010.

López-Yglesias, X., and Flagan, R. C.: Ion–Aerosol Flux Coefficients and the Steady-State Charge Distribution of Aerosols in a Bipolar Ion Environment, Aerosol Sci. Technol., 47, 688-704, 10.1080/02786826.2013.783684, 2013.

May, A. A., Levin, E. J. T., Hennigan, C. J., Riipinen, I., Lee, T., Collett, J. L., Jimenez, J. L., Kreidenweis, S. M. and Robinson, A. L.: Gas-particle partitioning of primary organic aerosol emissions: 3. Biomass burning, J. Geophys. Res. Atmos., 118(19), 11,327–11,338, doi:10.1002/jgrd.50828, 2013.

McMeeking, G. R., Kreidenweis, S. M., Baker, S., Carrico, C. M., Chow, J. C., Collett, J. L., Hao, W. M., Holden, A. S., Kirchstetter, T. W., Malm, W. C., Moosmüller, H., Sullivan, A. P. and Wold, C. E.: Emissions of trace gases and aerosols during the open combustion of biomass in the laboratory, J. Geophys. Res., 114(D19), D19210, doi:10.1029/2009JD011836, 2009.

Myhre, G., D. Shindell, F.-M. Bréon, W. Collins, J. Fuglestvedt, J. Huang, D. Koch, J.-F. Lamarque, D. Lee, B. Mendoza, T. Nakajima, A. Robock, G. Stephens, T. Takemura and H. Zhang: Anthropogenic and Natural Radiative Forcing. In: *Climate Change 2013: The Physical Science Basis. Contribution of Working Group I to the Fifth Assessment Report of the Intergovernmental Panel on Climate Change* [Stocker, T.F., D. Qin, G.-K. Plattner, M. Tignor, S.K. Allen, J. Boschung, A. Nauels, Y. Xia, V. Bex and P.M. Midgley (eds.)]. Cambridge University Press, Cambridge, United Kingdom and New York, NY, USA, 659-740, 2013.

Okoshi, R., Rasheed, A., Chen Reddy, G., McCrowey, C. J. and Curtis, D. B.: Size and mass distributions of ground-level sub-micrometer biomass burning aerosol from small wildfires, Atmos. Environ., 89, 392–402, doi:10.1016/j.atmosenv.2014.01.024, 2014.

Ontario Ministry of Natural Resources and Forestry. 2011 Forest Fire Summary. https://www.ontario.ca/law-and-safety/forest-fires. Accessed June 18, 2012.

Ortega, A. M., Day, D. A., Cubison, M. J., Brune, W. H., Bon, D., de Gouw, J. A. and Jimenez, J. L.: Secondary organic aerosol formation and primary organic aerosol oxidation from biomass-burning smoke in a flow reactor during FLAME-3, Atmos. Chem. Phys., 13(22), 11551–11571, doi:10.5194/acp-13-11551-2013, 2013.

Palmer, P. I., Parrington, M., Lee, J. D., Lewis, A. C., Rickard, A. R., Bernath, P. F., Duck, T. J., Waugh, D. L., Tarasick, D. W., Andrews, S., Aruffo, E., Bailey, L. J., Barrett, E., Bauguitte, S. J.-B., Curry, K. R., Di Carlo, P., Chisholm, L., Dan, L., Forster, G., Franklin, J. E., Gibson, M. D., Griffin, D., Helmig, D., Hopkins, J. R., Hopper, J. T., Jenkin, M. E., Kindred, D., Kliever, J., Le Breton, M., Matthiesen, S., Maurice, M., Moller, S., Moore, D. P., Oram, D. E., O'Shea, S. J., Owen, R. C., Pagniello, C. M. L. S., Pawson, S., Percival, C. J., Pierce, J. R., Punjabi, S., Purvis, R. M., Remedios, J. J., Rotermund, K. M., Sakamoto, K. M., da Silva, A. M., Strawbridge, K. B., Strong, K., Taylor, J., Trigwell, R., Tereszchuk, K. A., Walker, K. A., Weaver, D., Whaley, C., and Young, J. C.: Quantifying the impact of BOReal forest fires on Tropospheric oxidants over the Atlantic using Aircraft and Satellites (BORTAS) experiment: design, execution and science overview,

Atmos. Chem. Phys., 13, 6239-6261, doi:10.5194/acp-13-6239-2013, 2013.

Parrington, M., Palmer, P. I., Lewis, A. C., Lee, J. D., Rickard, A. R., Di Carlo, P., Taylor, J. W., Hopkins, J. R., Punjabi, S., Oram, D. E., Forster, G., Aruffo, E., Moller, S. J., Bauguitte, S. J.-B., Allan, J. D., Coe, H. and Leigh, R. J.: Ozone photochemistry in boreal biomass burning plumesParrington, M., Palmer, P. I., Lewis, A. C., Lee, J. D., Rickard, A. R., Di Carlo, P., … Leigh, R. J. (2013). Ozone photochemistry in boreal biomass burning plumes. Atmospheric Chemistry and Physics, 13, Atmos. Chem. Phys., 13(15), 7321–7341, doi:10.5194/acp-13-7321-2013, 2013.

Parrish, D. D., Stohl, A., Forster, C., Atlas, E. L., Blake, D. R., Goldan, P. D., Kuster, W. C. and de Gouw, J. A.: Effects of mixing on evolution of hydrocarbon ratios in the troposphere, J. Geophys. Res., 112(D10), D10S34, doi:10.1029/2006JD007583, 2007.

Petters, M. D. and Kreidenweis, S. M.: A single parameter representation of hygroscopic growth and cloud condensation nucleus activity, Atmos. Chem. Phys., 7(8), 1961–1971, doi:10.5194/acp-7-1961-2007, 2007.

Petters, M. D., Carrico, C. M., Kreidenweis, S. M., Prenni, A. J., DeMott, P. J., Collett, J. L. and Moosmüller, H.: Cloud condensation nucleation activity of biomass burning aerosol, J. Geophys. Res., 114(D22), D22205, doi:10.1029/2009JD012353, 2009.

Pierce, J. R., Chen, K. and Adams, P. J.: Contribution of primary carbonaceous aerosol to cloud condensation nuclei: processes and uncertainties evaluated with a global aerosol microphysics model, Atmos. Chem. Phys., 7, 5447–5466, 2007.

Reddington, C. L., Carslaw, K. S., Spracklen, D. V., Frontoso, M. G., Collins, L., Merikanto, J., Minikin, A., Hamburger, T., Coe, H., Kulmala, M., Aalto, P., Flentje, H., Plass-Dülmer, C., Birmili, W., Wiedensohler, A., Wehner, B., Tuch, T., Sonntag, A., O'Dowd, C. D., Jennings, S. G., Dupuy, R., Baltensperger, U., Weingartner, E., Hansson, H.-C., Tunved, P., Laj, P., Sellegri, K., Boulon, J., Putaud, J.-P., Gruening, C., Swietlicki, E., Roldin, P., Henzing, J. S., Moerman, M., Mihalopoulos, N., Kouvarakis, G., Ždímal, V., Zíková, N., Marinoni, A., Bonasoni, P. and Duchi, R.: Primary versus secondary contributions to particle number concentrations in the European boundary layer, Atmos. Chem. Phys., 11(23), 12007–12036, doi:10.5194/acp-11-12007-2011, 2011.

Reid, J. S., Hobbs, P. and Ferek, R.: Physical, chemical, and optical properties of regional hazes dominated by smoke in Brazil, J. Geophys. Res., 103(98), 32059–32080, DOI: 10.1029/98JD00458, 1998.

Reid, J. S., Hyer, E. J., Prins, E. M., Westphal, D. L., Zhang, J., Wang, J., Christopher, S. A., Curtis, C. A., Schmidt, C. C., Eleuterio, D. P., Richardson, K. A. and Hoffman, J. P.: Global Monitoring and Forecasting of Biomass-Burning Smoke: Description of and Lessons From the Fire Locating and Modeling of Burning Emissions (FLAMBE) Program, IEEE J. Sel. Top. Appl. Earth Obs. Remote Sens., 2(3), 144–162, doi:10.1109/JSTARS.2009.2027443, 2009.

Reid, J. S., Koppmann, R., Eck, T. F. and Eleuterio, D. P.: A review of biomass burning emissions part II: intensive physical properties of biomass burning particles, Atmos. Chem. Phys., 5(3), 799–825, doi:10.5194/acp-5-799-2005, 2005.

Rissler, J., Vestin, A., Swietlicki, E., Fisch, G., Zhou, J., Artaxo, P. and Andreae, M. O.: Size distribution and hygroscopic properties of aerosol particles from dry-season biomass burning in

674 Amazonia, Atmos. Chem. Phys., 6, 471–491, 2006.

675 Seinfeld, J. H. and Pandis, S. N.: Atmospheric chemistry and physics: from air pollution to climate
676 change, Hoboken, N. J., Wiley, 2006.

677 Spracklen, D. V., Carslaw, K. S., Pöschl, U., Rap, A. and Forster, P. M.: Global cloud condensation
678 nuclei influenced by carbonaceous combustion aerosol, Atmos. Chem. Phys., 11(17), 9067–9087,
679 doi:10.5194/acp-11-9067-2011, 2011.

680 Staudt, A. C., Jacob, D. J., Logan, J. A. and Sachse, G. W.: Continental sources , transoceanic
681 transport , and interhemispheric exchange of carbon, J. Geophys. Res., 106, 32571–32589, DOI:
682 10.1029/2001JD900078, 2001.

683 Taylor, J. W., Allan, J. D., Allen, G., Coe, H., Williams, P. I., Flynn, M. J., Le Breton, M., Muller, J. B.
684 A., Percival, C. J., Oram, D., Forster, G., Lee, J. D., Rickard, A. R. and Palmer, P. I.:
685 Size-dependent wet removal of black carbon in Canadian biomass burning plumes, Atmos. Chem.
686 Phys. Discuss., 14(13), 19469–19513, doi:10.5194/acpd-14-19469-2014, 2014.

687 Van der Werf, G. R., Randerson, J. T., Giglio, L., Collatz, G. J., Mu, M., Kasibhatla, P. S., Morton, D.
688 C., DeFries, R. S., Jin, Y. and van Leeuwen, T. T.: Global fire emissions and the contribution of
689 deforestation, savanna, forest, agricultural, and peat fires (1997–2009), Atmos. Chem. Phys.,
690 10(23), 11707–11735, doi:10.5194/acp-10-11707-2010, 2010.

691 Wiedensohler, A.: An Approximation of the Bipolar Charge-Distribution for Particles in the
692 Sub-Micron Size Range, J. Aerosol. Sci., 19, 387-389, 1988.

693 Wiedinmyer, C., Akagi, S. K., Yokelson, R. J., Emmons, L. K., Al-Saadi, J. A., Orlando, J. J. and Soja,
694 A. J.: The Fire INventory from NCAR (FINN): a high resolution global model to estimate the
695 emissions from open burning, Geosci. Model Dev., 4(3), 625–641, doi:10.5194/gmd-4-625-2011,
696 2011.

697 Yokelson, R. J., Crounse, J. D., Decarlo, P. F., Karl, T., Urbanski, S., Atlas, E., Campos, T. and
698 Shinozuka, Y.: Emissions from biomass burning in the Yucatan, Atmos. Chem. Phys., 5785–5812,
699 2009.

700

Table 1. Approximate physical transport age and distance of numbered flight transect midpoints from source fires. Ages were estimated by HYSPLIT back trajectories. The large ranges in the determined values are due to the large extent of the source fire region and variability in fire conditions. The distances are given from transect midpoints to the source fire region (± 150 km).

Transect #	Approx. physical Age [hrs]	Approx. distance from source [km]
Flight b622		
1	27 - 32	1450 - 1750
2	27 - 32	1350 - 1650
3	27 - 32	1250 - 1550
4	27 - 32	1150 - 1450
5	18 - 25	1050 - 1350
6	18 - 25	850 - 1150
7	18 - 25	850 - 1150
8	18 - 25	1050 - 1350
9	24 - 30	1350 - 1650
Flight b623		
1	24 - 36	1350 - 1650
2	28 - 36	2050 - 2350
3 - 4	28 - 36	1850 - 2150
5 - 6	28 - 36	1950 - 2250

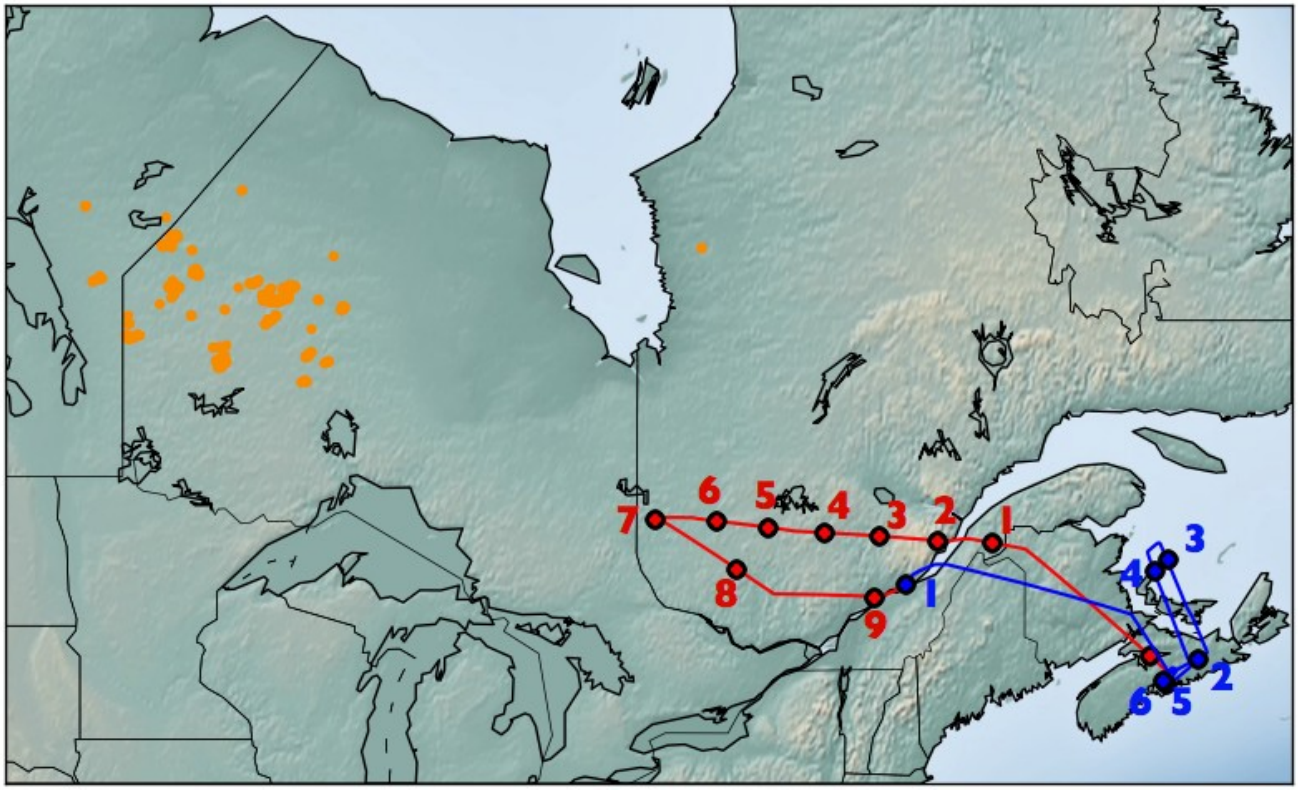

Figure 1. BORTAS-B ARA research flights b622 (red) from Nova Scotia to Quebec, and the return flight b623 (blue) both on July 20-21, 2011. Circles represent midpoints of ascent/descent transects along the flight paths. The ARA flew through biomass-burning emissions originating from fires in Northwestern Ontario. The July 17-20, 2011 MODIS hotspot fires (fire radiative power >100 MW) are plotted in orange.

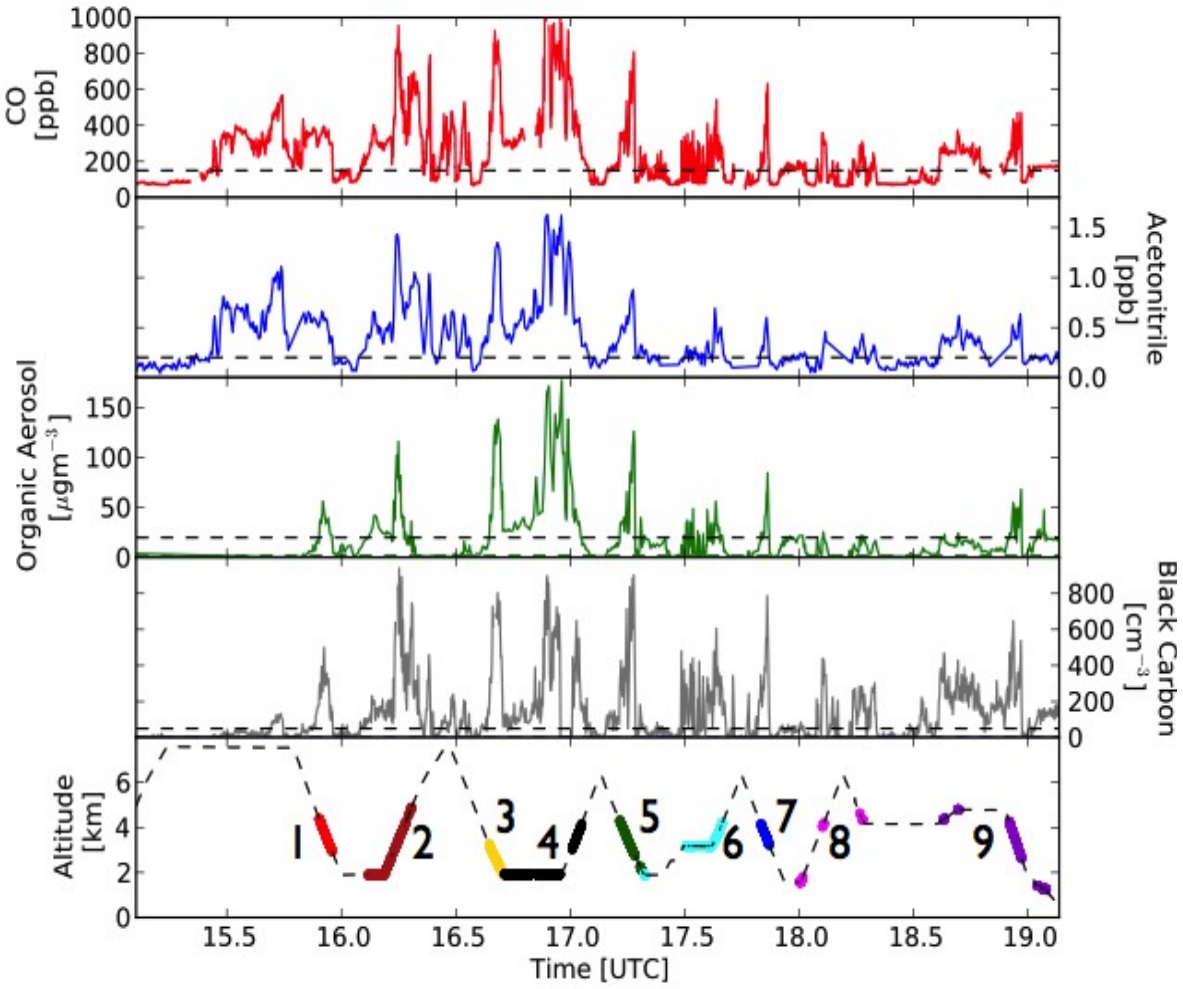

714 **Figure 2**. Time series of BORTAS-B aircraft measurements of biomass-burning tracer species for
715 Flight b622. Threshold values (dashed black lines) were used across four species as plume criteria: i)
716 CO (red, threshold = 150 ppb), ii) Acetonitrile (blue, threshold = 200 pptv), iii) Organic aerosols
717 (green, mass threshold= 20 μg m^{-3}, at STP), iv) Black carbon (grey, number threshold = 50 cm^{-3}, at
718 STP). The bottom panel shows flight altitude with plume sampling periods coloured. The plume data is
719 further divided into transects (1-9 in red-violet).

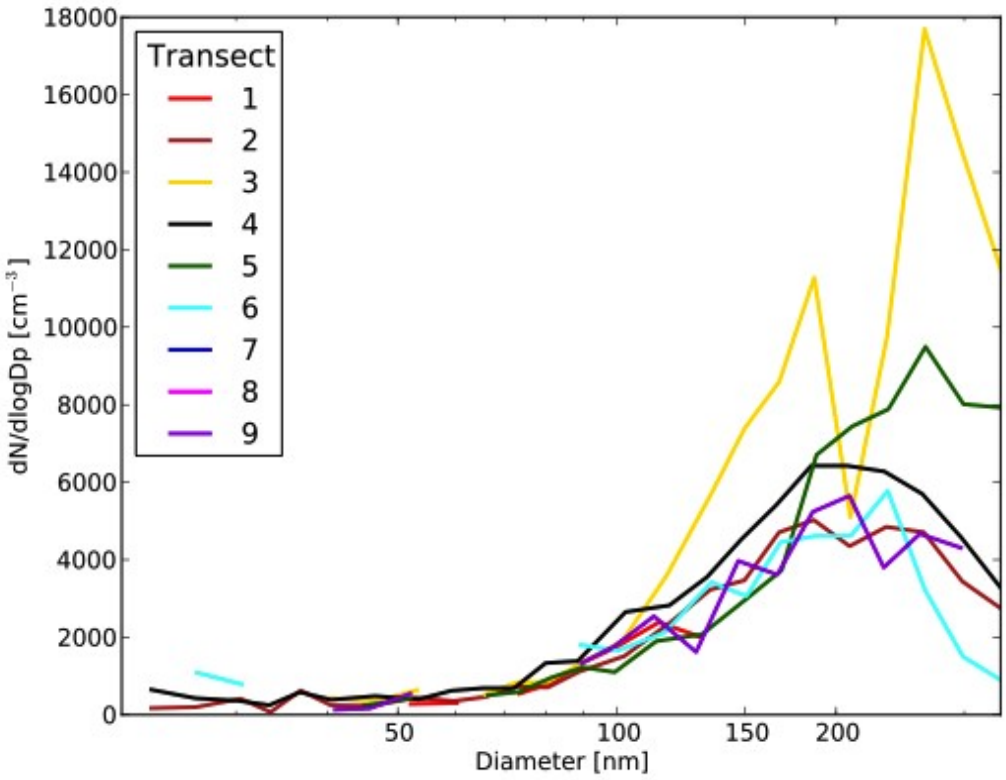

721 **Figure 3.** Median plume number size distributions (corrected to cm^{-3} at STP) divided by transect for
722 Flight b622. All size distributions show a consistent accumulation mode with D_{pm}~ 220 nm. Size bins
723 with less than three data points in any transect are not shown, limiting the contributions from transects
724 1, 7 and 8. The composite plume size-distribution for both Flight b622 and b623 is seen in Figure 5.

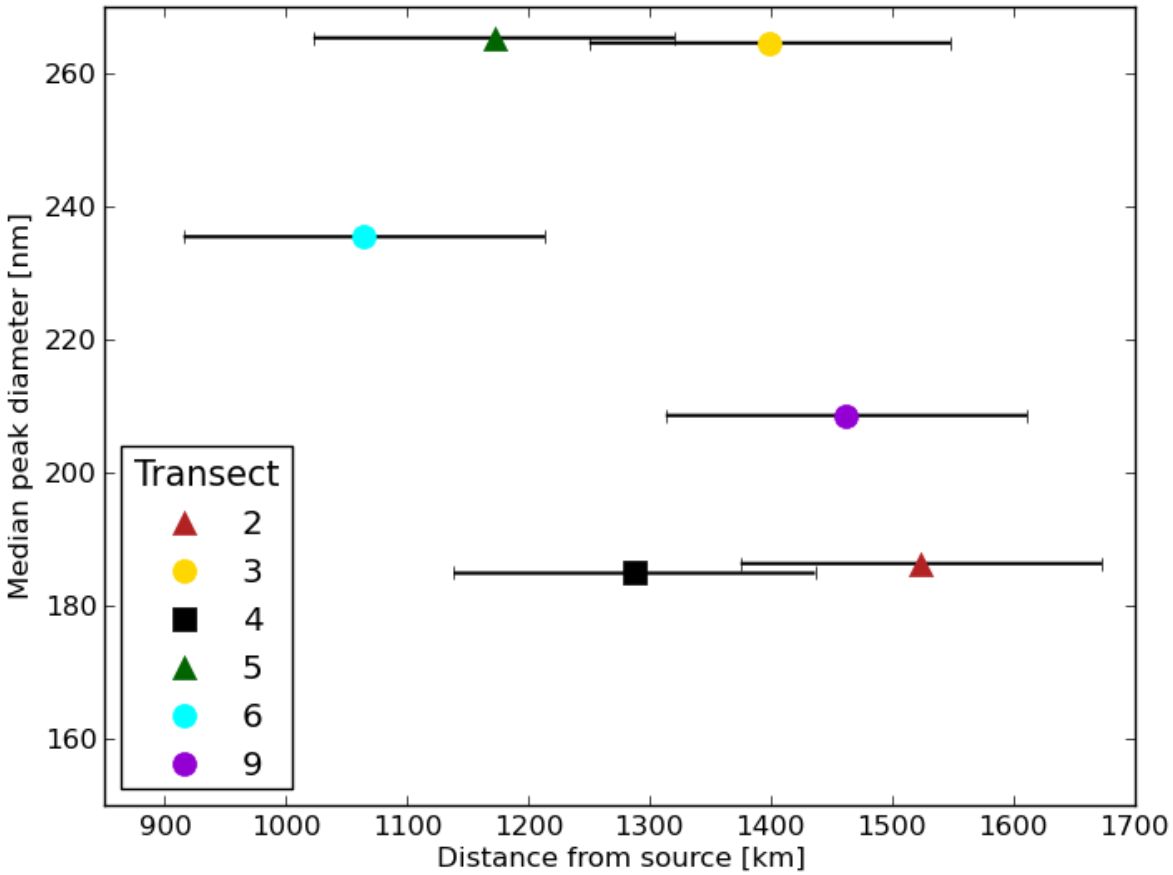

Figure 4. Accumulation mode peak diameter by transect (2-6, 9) showing no significant trend with plume transport distance. All colours are the same as in Figure 3. Distance from fire sources was estimated using transect midpoints and approximate source region area. Transects 1, 7 and 8 have insufficient accumulation mode plume data and have been omitted. The uncertainty bars show uncertainty in the distance from the source (± 150 km).

745

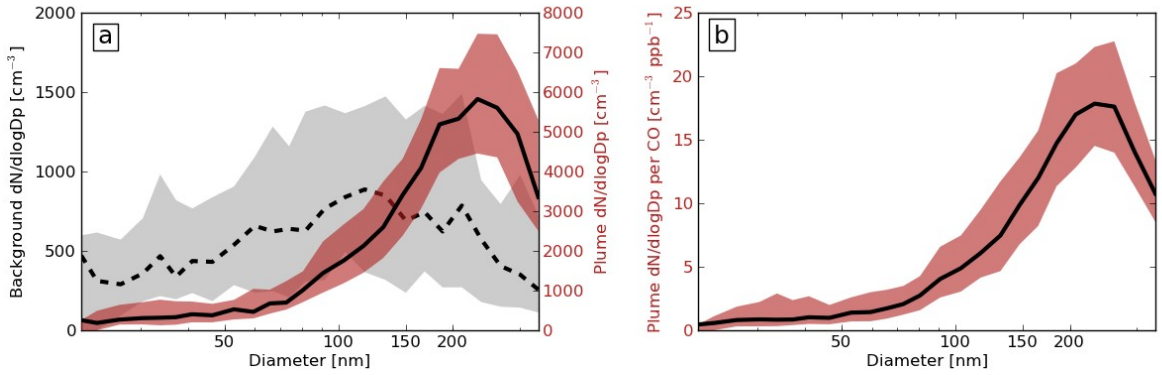

747

748

749 **Figure 5.** Composite median number size distributions for Flights b622 and b623 (cm^{-3} at STP). The
750 in-plume (red) and background (grey) air distributions are shown as absolute concentrations (5a). The
751 in-plume distributions are also normalized by CO mixing ratio (5b). The black lines are the median
752 with the 25th and 75th percentiles overlain. The plume distributions have D_{pm}= 230 nm.

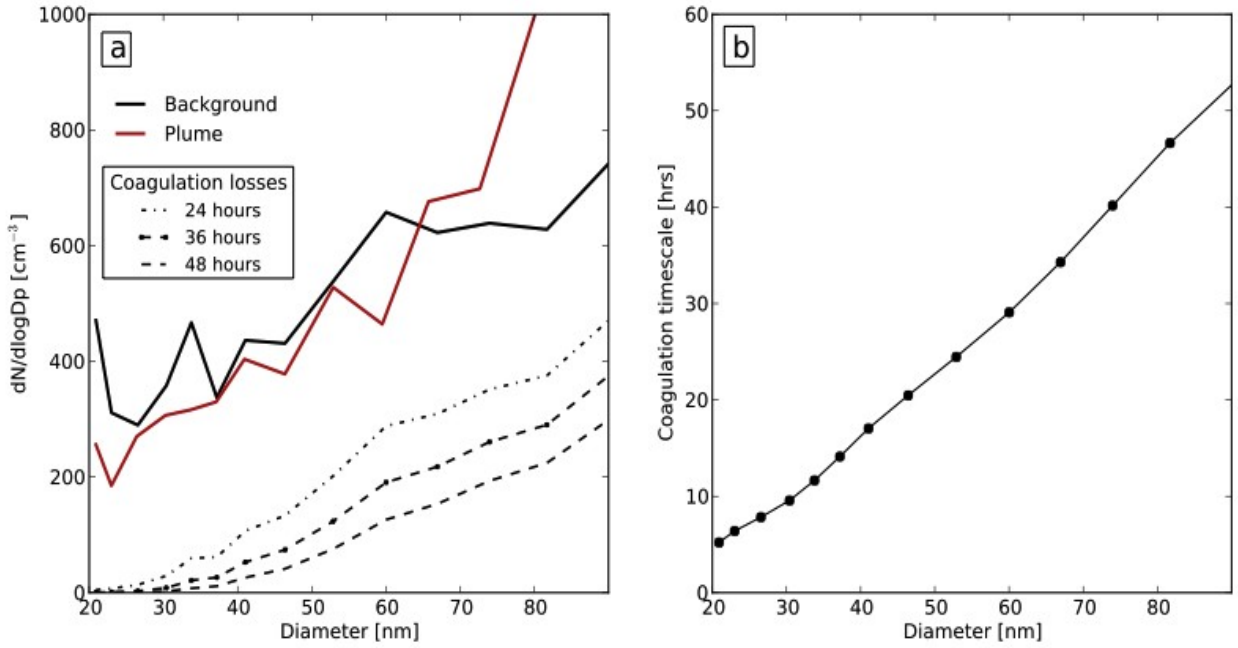

754 **Figure 6.** Figure 6a shows background (black solid line) and plume (red line) median concentrations
755 for small particle diameters (20-90 nm). The black dashed lines are the number distributions after 24,
756 36 and 48 hours of coagulational losses by the plume accumulation mode (Figure 5a) from the
757 background level concentrations. These calculated concentrations are much lower than those found in
758 plume. Figure 6b shows the coagulation lifetime as a function of particle diameter (on the order of 10s
759 of hours in this diameter range).

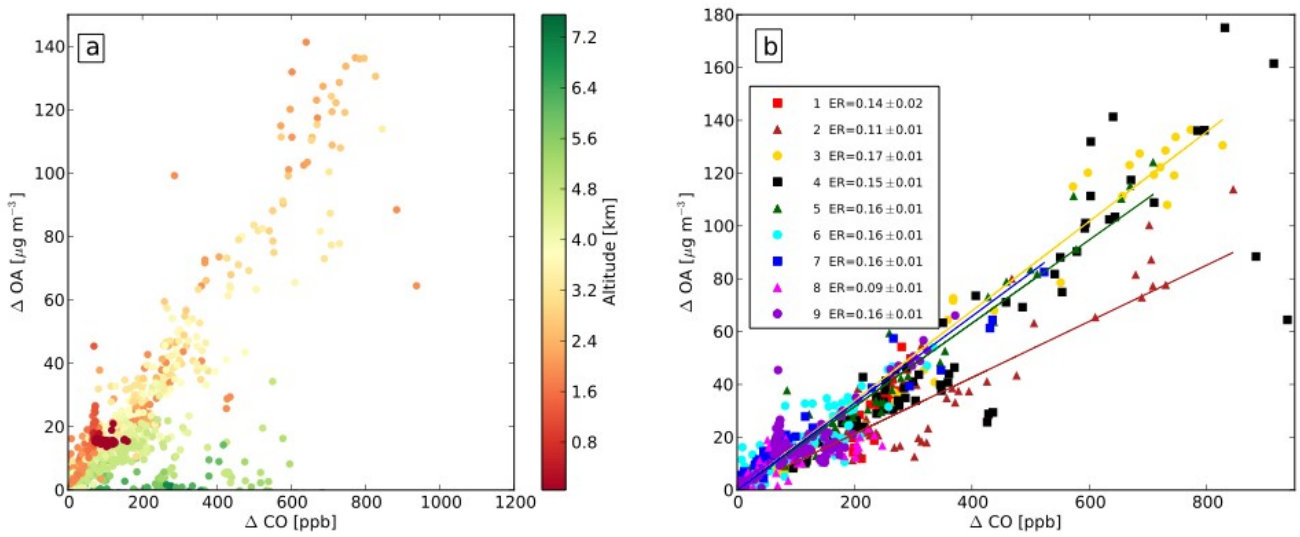

Figure 7. Enhancement ratios of ΔOA/ΔCO for Flight b622. Figure 7a is coloured by altitude showing potential aerosol washout in the high-altitude plume (>4.6 km). Figure 7b shows the ERs separated by flight transect showing individual enhancement ratios of between 0.09-0.17 ± 0.01 μg m^{-3} ppb^{-1} with generally high correlation coefficients (R^2>0.7) for the majority. The data points collected at altitudes greater than 4.6 km have been removed (as per 7a).

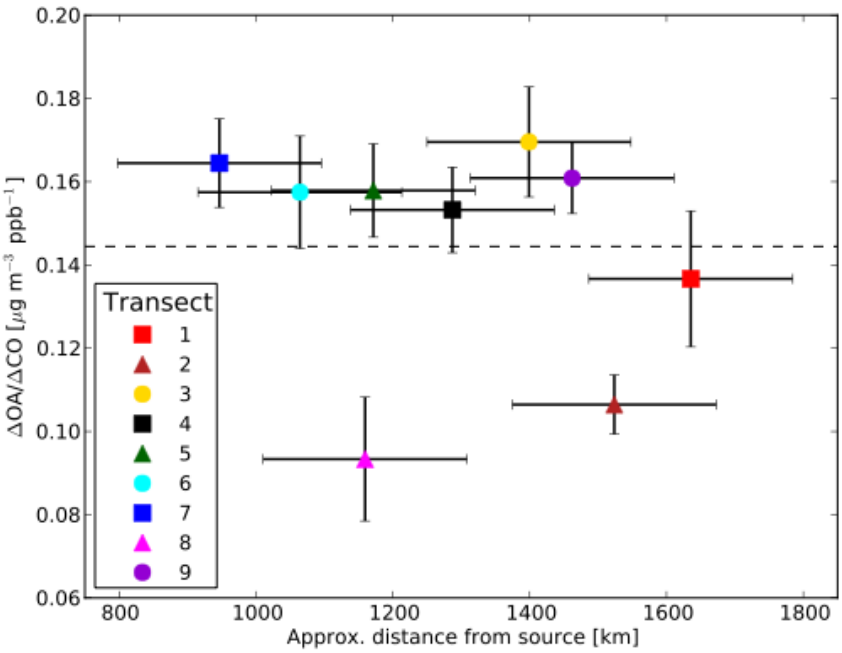

Figure 8. Transect ΔOA/ΔCO enhancement ratios for Flight b622 as a function of the distance from the source fire region. The average ER is represented by the dashed black line (0.144 μg m^{-3} ppb^{-1}). There is no discernible trend in ΔOA enhancement either by distance (x-axis) or time (colours). The uncertainty bars display the uncertainty in distance and in fitted enhancement ratios.

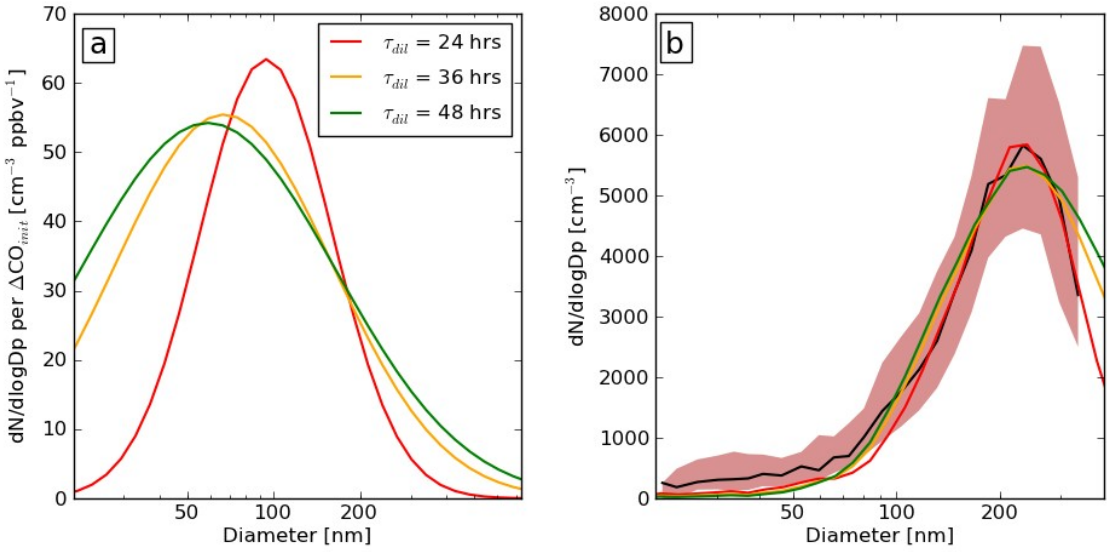

Figure 9. Figure 9a shows the optimized young-plume size-distributions for entrainment parameters τ_{dil}= 24, 36, 48 hrs as particle concentration per ΔCO_{init} [cm^{-3} ppbv-1]. Figure 9b shows the final modelled size-distributions compared to the measured aged plume size-distribution (black median, red quartiles).

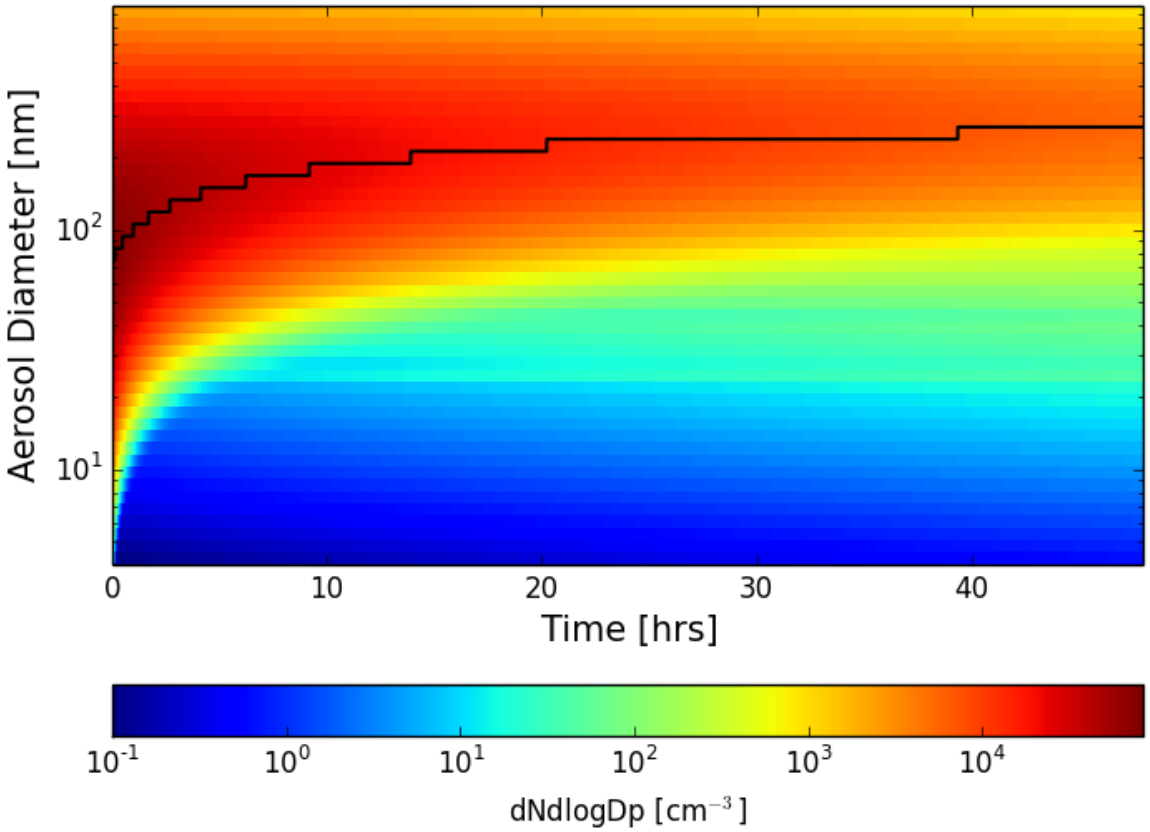

819 **Figure 10.** Plot of modelled size-distribution evolution for τ_{dil} = 36 hrs. The black line shows the peak
820 diameter at each timestep (Δt = 10s). The young-plume size-distribution has optimal initial parameters:
821 D_{pm}=67 nm, σ=2.4, N_0 = 80,000 cm^{-3}.